Faraday Discussions

ARTICLE

Molecular Self-Assembly of Substituted Terephthalic Acids at the Liquid/Solid Interface: Investigating the Effect of Solvent

Received 00th January 20xx,
Accepted 00th January 20xx

DOI: 10.1039/x0xx00000x

www.rsc.org/

A. Della Pia,[a] D. Luo,[a] R. Blackwell,[b] G. Costantini,[a] and N. Martsinovich[b]

Self-assembly of three related molecules – terephthalic acid and its hydroxylated analogues – at the liquid/solid interfaces (graphite/heptanoic acid and graphite/1-phenyloctane) has been studied using a combination of scanning tunnelling microscopy and molecular mechanics and molecular dynamics calculations. Brickwork-like patterns typical for terephthalic acid self-assembly have been observed for all three molecules. However, several differences became apparent: (i) formation or lack of adsorbed monolayers (self-assembled monolayers formed in all systems, with one notable exception of terephthalic acid at the graphite/1-phenyloctane interface where no adsorption was observed), (ii) the size of adsorbate islands (large islands at the interface with heptanoic acid and smaller ones at the interface with 1-phenyloctane), (iii) polymorphism of the hydroxylated terephthalic acids monolayers, dependent on the molecular structure and/or solvent. To rationalise this behaviour, molecular mechanics and molecular dynamics calculations have been performed, to analyse the three key aspects of the energetics of self-assembly: intermolecular, substrate-adsorbate and solvent-solute interactions. These energetic characteristics of self-assembly were brought together in a Born-Haber cycle, to obtain the overall energy effects of formation of self-assembled monolayers at these liquid/solid interfaces.

1. Introduction

The ability of molecules to self-assemble into extended ordered structures thanks to specific intermolecular interactions opens many possibilities for applications in such diverse fields as biomedicine[1, 2], molecular electronics[3-8], sensors[9] and catalysis.[10] In particular, by confining the self-assembly process on solid substrates, two-dimensional (2D) structures can be formed[11, 12] by exploiting a number of different intermolecular forces: from metal coordination[13, 14] to hydrogen bonding[14, 15], to weaker dispersion interactions.[16] While the nature of the interactions between the molecular units is typically the key factor in determining the resulting assembly, other more subtle influences have also been reported to affect the final supramolecular structures: the chemistry and symmetry of the substrate (even for inert surfaces such as highly ordered pyrolytic graphite (HOPG) and Au(111)[17]), the temperature,[18-20] the ultra-high vacuum (UHV) or solution environment,[19, 21, 22] the nature of the solvent,[19, 23-28] the concentration of the solute (the self-assembling molecule),[18, 29-35] and any co-adsorption of solvent or guest molecules[24, 25, 34, 36, 37]. The possibility of controlling supramolecular polymorphism by weak intermolecular interactions, such as interactions with the solvent, is a new and fascinating approach to the ultimate goal of rationally programming molecular self-assembly. However, its fundamental mechanisms are still not clearly understood, and it is likely that multiple mechanisms may be simultaneously at play: from co-adsorption of solvent and guest molecules[25, 31] to different solvation of small molecular aggregates – precursors to the extended self-assembly – in different solvents.[23]

In this work, we investigate the combined effects of the molecular structure and the nature of solvent in the molecular self-assembly of benzene dicarboxylic acids at the liquid/solid (HOPG) interface. In particular, we study the self-assembly of a series of three molecules: terephthalic acid (TPA) and its hydroxyl-substituted analogues 2-hydroxyterephthalic acid (2HTPA) and 2,5-dihydroxyterephthalic acid (25DHTPA), shown in **Figure 1.** Self-assembly of TPA has been widely studied on a variety of substrates (both inert, such as HOPG,[38-40] graphene,[41, 42] Au(111),[43] Ag(111)[44], Pt(111)[45] and reactive, such as Cu(100)[46, 47] and Cu(110),[48] Pd(111),[49] supported metallic multilayers,[50] doped Si(111),[44, 51] TiO_2,[52, 53] calcite[54]), and both in vacuum[41-44, 46, 48-54] and at the liquid/solid interface.[38-40] While on the more reactive surfaces TPA can undergo different transformations that modify its chemical structure (e.g. deprotonation of the carboxylic moieties), [46-48, 50, 52, 53] on inert substrates its self-assembly is characterised by the formation of molecular chains stacked in a brickwork fashion.[38-43] This supramolecular architecture is controlled by two types of interactions: intra-chain dimerisation of carboxylic groups to form strong hydrogen bonds (H-bonds) – as also observed for other carboxylic acid molecules: trimesic acid,[23, 30, 55] isophthalic

[a] Department of Chemistry, University of Warwick, Coventry, UK.
[b] Department of Chemistry, University of Sheffield, Sheffield, UK.

† Electronic Supplementary Information (ESI) available: Energies and structures for force field fitting, schematic of a 2D unit cell and lattice parameters, potential energy surfaces for 2D self-assembly of TPA, 2HTPA and 25DHTPA. See DOI: 10.1039/x0xx00000x

acid,[40] 1,3,5-benzenetribenzoic acid[24] stilbenedicarboxylic acid[56] – and secondary inter-chain dispersion interactions.

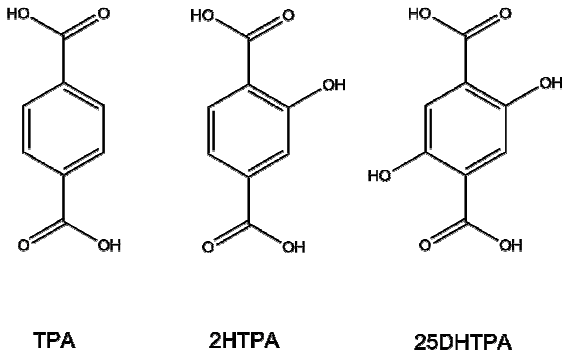

Figure 1 Structures of (a) terephthalic acid (TPA), (b) 2-hydroxyterephthalic acid (2HTPA) and (c) 2,5-dihydroxyterephthalic acid (25DHTPA).

Here we introduce additional "lateral" OH moieties and vary their number to tune the inter-chain interactions and to study their effect on the self-assembly. We also use two different solvents: a nonpolar solvent, 1-phenyloctane (PO), and a polar solvent with an acid group, heptanoic acid (7A), to investigate the effect of solvent-solute interactions (π-stacking vs H-bonds) on the assembly.

We use a combination of scanning tunnelling microscopy (STM) experiments and molecular mechanics (MM) and molecular dynamics (MD) calculations. The STM results reveal similarities in the 2D structures formed by these molecules, but also differences: (i) different surface coverage by adsorbates at the two liquid/solid interfaces, (ii) formation of two slightly different self-assembled structures of 25DHTPA depending on the solvent, and (iii) co-existence of several domains with different molecular orientations for the asymmetric 2HTPA molecule. Computational modelling is used to rationalise the observed 2D structures and the equilibrium between molecules in solution and self-assembled monolayers at the liquid/solid interface. Similar to what done in previous related work[39, 56], Born-Haber cycles are constructed to evaluate the energy gain upon formation of self-assembled monolayers from solution.

2. Methods

2.1. Experimental Methods

A fresh graphite surface was obtained by cleaving a HOPG crystal (grade ZYB) with Scotch tape before each molecular deposition. A saturated solution was prepared by dissolving the molecules in the solvent (heptanoic acid or 1-phenyloctane) in a small glass vial; approximately 10-30µL of the solution were then deposited on the HOPG substrate using a micropipette.

The adsorbed self-assembled 2D molecular structures were characterised using STM (Veeco with Nanoscope E controller and an A-type scanner) operating in ambient conditions at the solid-liquid interface, and using mechanically-sheared Pt/Ir (90/10) tips. For molecular imaging, the bias voltage (applied to the sample) ranged from −1.5 to 1.0 V, with typical currents between 70 and 100 pA. For atomic resolution imaging of the underlying HOPG surface, typical tunnelling parameters were −0.1/0.1 V and 100-800 pA. All STM images were processed using the WSxM software.[57] STM images which have been recalibrated by using half-half images containing both atomic resolution of the HOPG substrate and the molecular layer[55] are indicated as "rescaled STM images" in the figure captions.

2.2. Computational Methods

Force field. The calculations of the 2D assembly of the TPA, 2HTPA and 25DHTPA molecules, adsorption of these molecules and solvent molecules on graphite, adsorption of the solvent on 2D molecular monolayers, and solvation of these molecules by liquid solvent were carried out using molecular mechanics, with the Tinker software[58] and the MM3 force field.[59, 60] The force field parameters for the H-bonding in the carboxylic acid dimer (interactions between carboxylic hydrogen, atom type 24, and double-bonded carboxylic oxygen, atom type 77) were taken from our previous work Ref.[61]: the energy parameter $\varepsilon_{24\cdots77}$= 7.78 kJ mol^{-1} and the distance parameter $r_{24\cdots77}$ = 1.75 Å.

The 2HTPA and 25DHTPA molecules contain additional phenolic hydroxyl groups, and therefore different types of H-bonding interactions, both intra- and intermolecular, are expected between two hydroxyl groups and between hydroxyl and carboxylic groups (see **Table 1**). H-bonding parameters for these interactions are not available in MM3 (except for the interaction type 73-6: hydroxyl hydrogen – phenolic oxygen). Therefore, accurate quantum-chemistry calculations were performed using Moller-Plesset perturbation theory (MP2)[62] and were used to fit the missing H-bonding parameters. Four isomers of 2HTPA were considered, with different positions and conformations of the hydroxyl group relative to the carboxylic groups, as well as several 2HTPA and phenol dimers with a range of hydroxyl-hydroxyl and hydroxyl-carboxyl arrangements (see Electronic Supporting Information (ESI), Section S1). MP2 calculations with the DZVP basis set were done using Gaussian09[63] software; all binding energies were corrected for the basis set superposition error (BSSE). Some of the calculations were also done with the larger TZVP basis set but the resulting binding energies and relative energies of isomers were similar to what was obtained with the DZVP basis set within 2.5 kJ mol^{-1}). MM3 calculations were then done on the same systems, while varying the energy and distance parameters for each interaction, to achieve a good fit both in terms of energies (within 5.0 kJ mol^{-1}, see ESI Section S1) and geometries (within 0.2 Å). The best parameters, shown in **Table 1**, were used for all the following MM calculations.

Table 1. Hydrogen bonding parameters for the MM3 force field, fitted in this work

Interaction (H...O)	Atom types	$r_{H...O}$, Å	$\varepsilon_{H...O}$, kcal mol^{-1}
$H_{(carboxyl)}...O=_{(carboxyl)}$	24-77 (Ref.[61])	1.75	7.78
$H_{(phenol)}...O=_{(carboxyl)}$	73-77	1.75	7.78
$H_{(phenol)}...OH_{(carboxyl)}$	73-75	1.9	5.5
$H_{(phenol)}...OH_{(phenol)}$	73-6	2.3	3.2
$H_{(CH)}...OH_{(phenol)}$	5-6	2.6	1.0

Calculations of 2D structures. 2D monolayer structures of 2HTPA and 25DHTPA were explored by scanning through combinations of their 2D lattice parameters. First, isolated 1D molecular chains were modelled: the lattice parameter *a* (along the molecular chain) was varied, with a step of 0.1 Å, to find the lowest-energy value of *a*. Then, while keeping *a* fixed at its optimum value, 2D arrangements of the molecular chains were modelled by simultaneously varying the parameters b_y (perpendicular distance between the chains) and b_x (the shift of the chains relative to each other along the chain direction, shown schematically in **Figure 2**), with a step of 0.1 Å, similar to the procedure used in Ref.[39] The parameters b_x and b_y are directly related to the parameters *b* ($b^2 = b_x^2 + b_y^2$) and γ ($\sin\gamma = b_y / b$) typically used to describe 2D lattices. The structures were kept planar by fixing the z coordinates of all atoms. The 2D potential energy surfaces (PES) obtained by varying b_x and b_y were analysed to identify the energy minima.

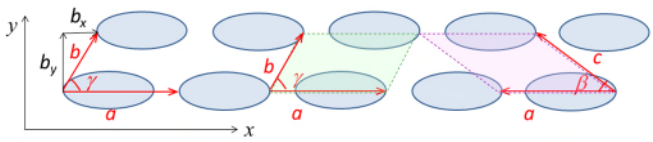

Figure 2 Schematic showing (left) the definition of the lattice parameters *a* and *b* and the angle γ between them, and decomposition of *b* into the components b_x (intermolecular separation along the direction of the chain – along the *x* axis) and b_y (inter-chain separation – along the *y* axis); (middle and right) two choices of the inter-chain lattice parameter, *b* or *c* (and the corresponding angles γ and β) for the same lattice, leading to unit cells of different shapes but same size.

Calculations of adsorption. A large hydrogen-terminated graphene sheet (20×20 C atoms) was used to model the adsorption of the three terephthalic acid molecules and of the solvent molecules, on HOPG. All atoms of the graphene sheet and the lateral coordinates (*x* and *y*) of the adsorbates were fixed, while the vertical coordinates of the adsorbates were allowed to optimise. A 2D grid of adsorption positions above the graphene sheet was considered, covering the rectangular shaped graphene unit cell (2.46 × 4.26 Å, with step 0.2 Å). Adsorption of single solvent molecules above TPA and substituted TPA monolayers was modelled similarly: all atoms in the monolayer were fixed, and the lateral coordinates of only the first and last atoms of the solvent's alkyl chains were fixed, thus allowing the solvent molecules the flexibility to adjust their conformation (this flexibility was found not necessary on graphene, where the adsorbates' conformations remained essentially unchanged). As with the direct adsorption on graphene, a 2D grid of adsorption positions above the monolayers was considered, covering the whole area of each monolayer's unit cell, with step 0.2 Å.

Calculations of solvation. Molecular dynamics simulations were used to obtain solvation energies of TPA, 2HTPA and 25DHTPA in 7A and PO. To achieve good sampling of the solvent and solute-in-solvent systems, several 3D boxes of solvent were constructed, with periodic boundary conditions: a parallelepiped-shaped box containing 200 7A molecules and a roughly cubic box containing 192 7A molecules, a parallelepiped-shaped PO box containing 192 PO molecules and a roughly cubic box containing 198 PO molecules. Cell volumes were chosen to reproduce the experimental densities of these solvents: 0.918 g cm^{-3} (7A) and 0.858 g cm^{-3} (PO). Solvent systems were first annealed from 1000 K to 298 K for 1 ns, then MD simulations using the canonical (NVT) ensemble were run until variation in energies (averaged every 0.5 ns) was less than 5 kcal mol^{-1} (this took 2-3 ns for PO and 4-6 ns for 7A, since hydrogen bonding of carboxylic groups takes a longer time to equilibrate). The Nose-Hoover thermostat was used; the integration time step was 1 fs; the "rattle" algorithm was used to constrain all covalent bonds to H atoms to their ideal bond length. 6 simulations of PO solvent and 10 simulations of 7A solvent were run, and energies (collected over the last 1 ns) were averaged over these MD runs.

To create solvent-solute systems, one or two molecule of the solvent was removed and replaced by one or two molecule of the solute. The volume of the cell was adjusted, to account for the different molecular volume of the solute compared to the solvent (the molecular volumes were calculated from the molar masses and densities: TPA, 1.52 g cm^{-3};[64] 2HTPA, 1.61 g cm^{-3};[65] 25DHTPA, 1.779 g cm^{-3};[66] 7A, 0.918 g cm^{-3};[67] PO, 0.858 g cm^{-3} [68]). One solute molecule per 192–200 solvent molecules corresponds to the solute concentrations of ~0.035 mol dm^{-3} in 7A and ~0.023 mol dm^{-3} in PO. Several solvent-solute cells were built and simulated: 9 for TPA in 7A, 6 for 2HTPA and 25DHTPA in 7A and 6 for each solute molecule in PO. Solute-7A systems were initially annealed from 400 to 298 K for 1 ns; then all solute-solvent systems were simulated using MD (NVT ensemble) until the averaged energy variation was below 5 kcal mol^{-1}. Similar to the pure solvents, solute in PO took less time to equilibrate (2-4 ns) than in 7A (3-7 ns). The last 1 ns of each MD simulation were used to determine the energies of solute in solvent.

3. Results and Discussion

3.1. STM imaging

STM images of TPA, 2HTPA and 25DHTPA, obtained at the interface of HOPG with 7A and PO solutions, are shown in **Figures 3** and **4**, demonstrating that in most cases the molecules formed ordered self-assembled layers. One notable exception is TPA in PO, where no self-assembled monolayer was observed, as discussed below.

The measured lattice parameters for all observed monolayers are summarised in **Table 2**. The images show many similarities: the molecules are imaged as bright spots corresponding to the benzene rings, sometimes with submolecular contrast; all observed monolayers have a brickwork-like pattern, indicative of the formation of chains held together by strong intra-chain interactions (dimeric hydrogen bonds) and weak inter-chain interactions.[40, 61] The measured lattice parameters for TPA at the HOPG/7A interface (a = 10.0 Å, b = 7.7 Å, γ = 48°, relative error ±5%) are in good agreement with previous studies of TPA self-assembled monolayers on a variety of substrates (HOPG, graphene, Au(111), Pt(111)), both at the liquid/solid interface and in UHV[38-41, 43, 45] as shown in **Table 3**.

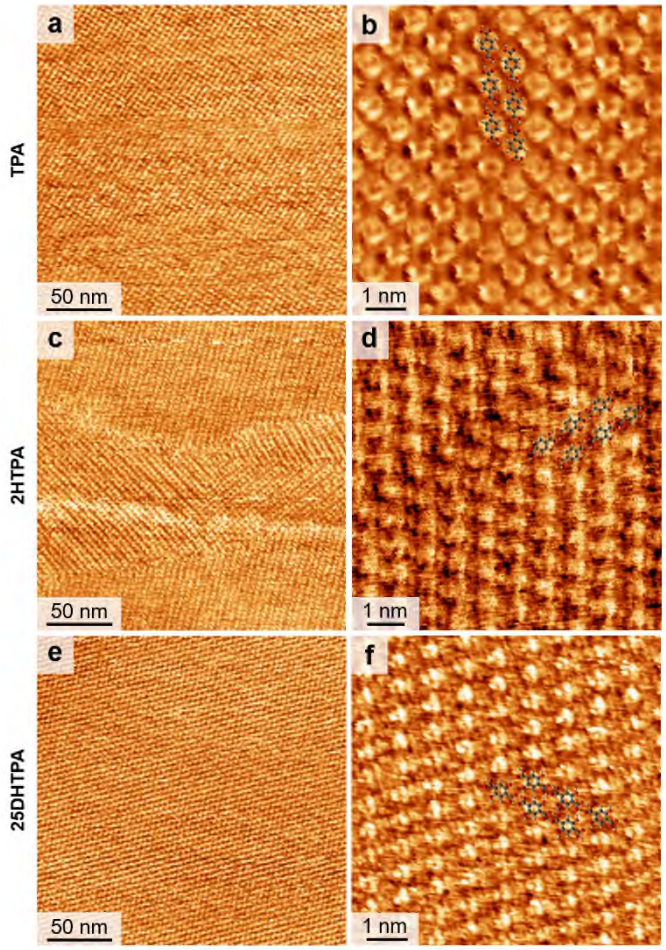

Figure 3. STM images of self-assembled monolayers at the HOPG/7A interface: (a, b) TPA; (c, d) 2HTPA; (e, f) 25DHTPA. Overlays of molecular structures in (b, d, f) show proposed supramolecular arrangements in these 2D structures. (b, d, f) are rescaled STM images.

Figure 4. STM images of self-assembled monolayers at the HOPG/PO interface: (a, b) TPA; (c, d) 25DHTPA. Overlays of molecular structures in (b, d) show proposed supramolecular arrangements in these 2D structures. (b, d) are rescaled STM images.

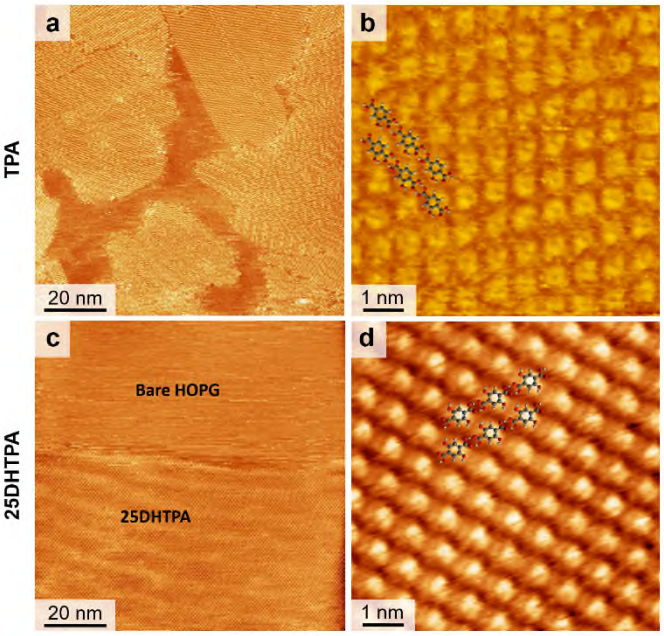

Table 2. Experimental lattice parameters of TPA, 2HTPA (only regular brickwork assembly) and 25DHTPA monolayer structures from STM measurements (the relative uncertainty is 5% in all cases)

Molecule	Solvent	a / Å	b / Å	γ / °	Area / Å molecule^{-1}
TPA	7A	10.0	7.7	48	57.2
2HTPA	7A, PO	9.4	8.4	50	60.5
25HTPA	7A	9.3	8.6	44	55.6
25HTPA	PO	9.3	8.4	57	65.5

Table 3. Comparison of TPA lattice parameters obtained in this work with literature values for 2D monolayers of TPA on inert and weakly reactive substrates and for TPA bulk crystal.

Source	Substrate	Solvent or UHV	a / Å	b / Å	γ / °
This work	HOPG	7A	10.0±0.5	7.7±0.4	48±2
Ref.[38]	HOPG	7A	10.0	7.5	60
Ref.[40]	HOPG	7A	9.8	7.4	60
Ref.[39]	HOPG	9A	9.6±0.1	7.8±0.1	50±1
Ref	graphene	7A	9.5±0.2	7.6±0.6	53±3
Ref.[41]	graphene	UHV	9.8±0.6	7.4±0.3	60
Ref.[43]*	Au(111)	UHV	10.0±0.3	7.3±0.3	55±3
Ref.**	Cu(111)	UHV	9.5±0.1	N/A	N/A
Ref.[45]	Pt(111)	UHV	9.6	7.3	49
Ref.[49]***	Pd(111)	UHV	9.5±0.6	N/A	N/A
Ref.[69]	3D crystal	-	9.54	7.73	43

* Averaged over three distinct sets of a, b, γ for three non-equivalent directions on the reconstructed Au(111) surface
** Averaged over two main a values.
*** Value for 1D chains (2D monolayers of *deprotonated* molecules were also observed)

However, there are also notable differences between the monolayers formed in the two solvents. When deposited from 7A, all three molecules form ordered extended islands and completely cover the HOPG surface (**Figure 3**). In contrast, with the PO solvent, the molecules tend to form isolated islands rather than a complete monolayer (**Figure 4**). In the case of TPA in PO, the molecules do not adsorb at all: no molecules were observed on the HOPG surface despite extensive scanning.

The overview of the TPA lattice parameters obtained in this study and reported in the literature (**Table 3**) shows that the structure of the monolayers formed by TPA is essentially unchanged on all inert substrates, both at the solid/liquid interface and in the UHV environment; therefore, the lack of adsorption at the HOPG/PO interface is unexpected. However, previous studies of TPA self-assembly were done only in UHV and in alkanoic acid (heptanoic acid[38, 40] and nonanoic acid [39]) solvents; we are not aware of this molecule having been adsorbed from phenyloctane or other nonpolar solvent. There is, however, an example of a chemically similar system for which no adsorbed self-assembled layers were observed: phthalic acid at the HOPG/7A interface[40] – attributed to weak adsorption of this non-planar molecule on HOPG. In our case of TPA, the likely difference is the nature of solvation: hydrogen bonding interaction of TPA with 7A, against π-stacking in PO. The lack of TPA adsorption suggests strong π-stacking interaction with the PO solvent, which competes with the molecule-substrate interaction and limits the formation of an adsorbed layer.

Comparing the assembly of the symmetric molecules (TPA and 25DHTPA) to the asymmetric 2HTPA molecule, it can be observed that while the former arrange into extended islands with only one orientation with respect to the HOPG lattice (**Figure 3a**, **b**, **e**, **f** and **Figure 4c**, **d**), the latter forms several molecular domains with different orientations, both in 7A and PO (**Figure 3c**, **d** and **Figure 4a**, **b**). This can be attributed to the existence of different adsorption orientations for the 2HTPA molecule – with different domains containing molecules with the different orientations. The solvent affects the 2HTPA island size but not the molecular packing: the same brickwork-like structure with very similar lattice parameters (see **Table 2**) is seen for both solvent interfaces. The *b* parameter (describing the inter-chain distance) and the angle γ are slightly larger in 2HTPA than in TPA, indicating that 2HTPA chains are more widely spaced than TPA chains. This is clearly caused by the presence of the hydroxyl moiety in 2HTPA: the bulkier OH groups and the repulsion between oxygens in hydroxyl and carboxyl groups in neighbouring chains are likely to both play a role here. Surprisingly, the distance along the chain, i.e. along the hydrogen-bonded carboxylic groups, is reduced compared to TPA, from 10.0 to 9.4 Å. A possible reason for this may be the effect of the substrate, i.e. the relationship between the substrate periodicity and the intra-chain periodicity,[70] and the possibility of inter-chain interactions (either weak or strong, depending on the presence of OH groups) modulating the substrate interactions.

A closer inspection of the 2HTPA images reveals that, besides regions characterised by a *regular* brickwork assembly (**Figures 3c** and **d** and **Figures 4a** and **b**), also other regions exist displaying an alternative assembly with a high variability in the inter-chain separation, noticeable as gaps between the chains (**Figure 5**). This second type of assembly develops at the interface with both 7A and PO. While the inter-chain distance in the regular 2HTPA structure is 8.4 $\pm$ 0.4 Å, the other regions show a pairing of chains with alternating short (7.2-7.4 Å) and long (9.1-9.2 Å) separations and are therefore dubbed *alternating* 2HTPA assembly. The likely explanation for these enlarged and shortened inter-chain distances is the repulsion between hydroxyl groups of adjacent 2HTPA molecules. Notably, the shorter inter-chain separation approaches the corresponding value in TPA (7.7 Å). It is thus likely that in the regular brickwork regions (**Figures 3c** and **d** and **Figures 4a** and **b**) the 2HTPA molecules have the OH groups all oriented in the same direction forming evenly spaced single chains (as shown schematically in **Figure 6a**), while in the alternating assembly (**Figure 5**), molecules with OH facing/opposing each other belong to chains with wider/smaller separations (**Figure 6b**). Thus, 2HTPA displays polymorphism, which is not caused by the solvent but rather originates from the structure of the molecules themselves.

Figure 5. STM images of the alternating 2HTPA assembly: (a, b) at the

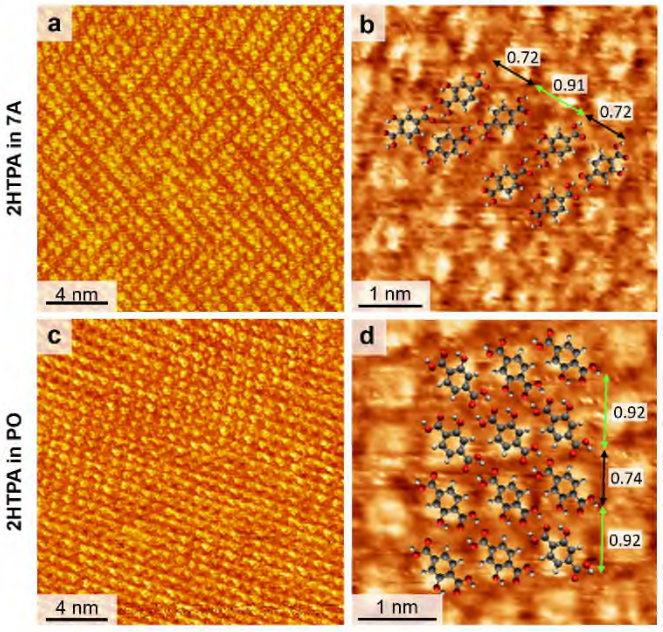

HOPG/7A interface; (c, d) at the HOPG/PO interface. Overlays of molecular structures in (b, d) show proposed supramolecular arrangements in these 2D structures, while numbers show measured inter-chain separations in nm. (b, d) are rescaled STM images.

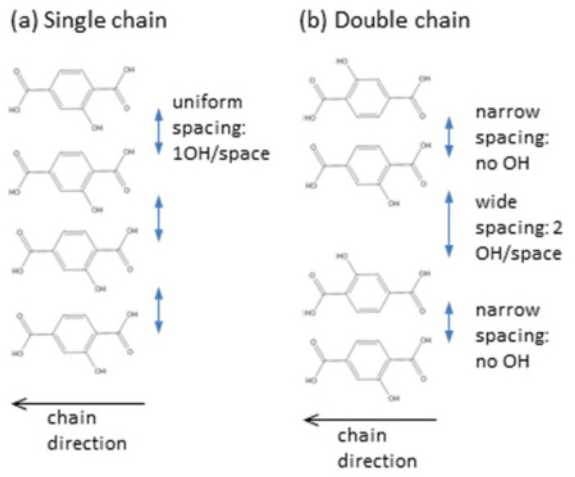

Figure 6. Schematics of two possible types of arrangements of 2HTPA molecules in 2D periodic structures: (a) single chain structure: all 2HTPA molecules have the same orientation of the OH groups, resulting in uniform inter-chain spacing; (b) double chain structure: pairs of 2HTPA chains with alternating OH orientations, resulting in two different inter-chain spacings.

25DHTPA (**Figures 3e** and **f** and **Figures 4c** and **d**) also forms a brickwork structure, similar to TPA and 2HTPA. However, in this case there are quantitative differences between the structures formed at the interfaces with 7A and in PO (see **Table 2**): although the values of the *a* and *b* lattice parameters are very similar for both solvents, the angle γ between them is noticeably larger in PO (57°) than in 7A (44°). Thus, the structure formed at the interface with PO is 18% less densely packed than the structure formed at the interface with the 7A solvent, with the difference likely being caused by different orientations of hydroxyl groups. Thus, 25DHTPA monolayers display solvent-induced polymorphism.

To summarise, all three terephthalic acid molecules showed differences in their self-assembly behaviour at the two studied solid-liquid interfaces: presence or absence of self-assembled monolayers at the solid-liquid interface (TPA); full or partial surface coverage of the molecular layers (2HTPA, 25DHTPA); singly oriented (TPA, 25DHTPA) or multiply oriented (2HTPA) molecular domains; co-existence of two polymorphs for both solvents (2HTPA); formation of two polymorphs depending on the solvent (25DHTPA). Theoretical insight is necessary in order to understand the origin of these differences and will be presented in the next section.

3.2. Calculations of 2D structures of 2HTPA and 25HTPA

The whole "surface-adsorbate-solvent" system is too large to be modelled efficiently at once. However, it can be partitioned into key components: (i) 2D self-assembled monolayers (intermolecular interactions), (ii) individual molecules adsorbed on the graphite surface (molecule-substrate interactions) and (iii) solute molecules surrounded by solvent (solute-solvent interactions).

To understand the differences in the self-assembly and the polymorphism of 2HTPA and 25DHTPA molecules, calculations of their 2D periodic structures in isolation (i.e. without substrate and solvent) were done using MM, as described in the Computational Methods section. To identify all possible stable 2D arrangements of these molecules, potential energy surfaces (PES) were obtained by scanning through combinations of the 2D lattice parameters. The monolayer structures (**Table 4**) were compared to TPA results published earlier[39, 61] and to the experimental results found in this work.

Table 4. Calculated lattice parameters, area per molecule and monolayer binding energies (relative to an isolated molecule) of low-energy 2D monolayers of TPA, 2HTPA and 25DHTPA. The calculated values for TPA from Ref.[39] are included for comparison.

Molecule	2D arrangement	E_{ML} / kJ mol^{-1}	*a* / Å	b_1; b_2 / Å	c_1; c_2 / Å	α_1, α_2 / °	β_1; β_2 / °	γ_1; γ_2 / °	Area / Å^2 molecule^{-1}	Assignment to experimental structures
TPA	Ref.[39]	−76.8	9.38	8.1; –	7.3; –	75.1; –	56.4; –	49; –	56.83	Regular TPA
2HTPA	SC-Min1	−79.0	9.4	7.5; –	8.0; –	74; –	51; –	55; –	58.28	Regular 2HTPA (?)
2HTPA	DC1-Min1	−82.6	9.4	7.3; 7.5	8.3; 7.9	77; 75	49; 51	58; 54	57.81	Regular 2HTPA
2HTPA	DC1-Min2	−82.3	9.4	7.5; 8.8	8.3; 7.2	73; 71	50; 62	58; 46	59.69	Alternating 2HTPA
2HTPA	DC1-Min3	−78.6	9.4	6.8; 8.1	11.1; 7.3	59; 75	39; 56	82; 49	60.16	–
2HTPA	DC2-Min1	−81.0	9.4	7.0; 6.9	11.5; 8.3	52; 76	36; 59	88; 59	60.63	–
2HTPA	DC2-Min2	−78.2	9.4	8.7; 7.0	7.1; 8.7	72; 73	62; 45	46; 62	58.28	Alternating 2HTPA (?)
2HTPA	DC3-Min1	−79.1	9.4	7.4; 7.8	9.5; 7.5	66; 76	46; 53	68; 51	60.63	–
25HTPA	SC-Min1	−90.1	9.4	7.3; –	8.3; –	74; –	48; –	58; –	58.28	25DHTPA in 7A
25HTPA	DC-Min1	−82.2	9.4	7.4; –	9.3; –	67; –	47; –	66; –	63.45	25DHTPA in PO
25HTPA	DC-Min2	−81.9	9.4	9.5; 7.4	7.4; 9.6	66; 66	68; 46	46; 68	64.39	–

Faraday Discussions

ARTICLE

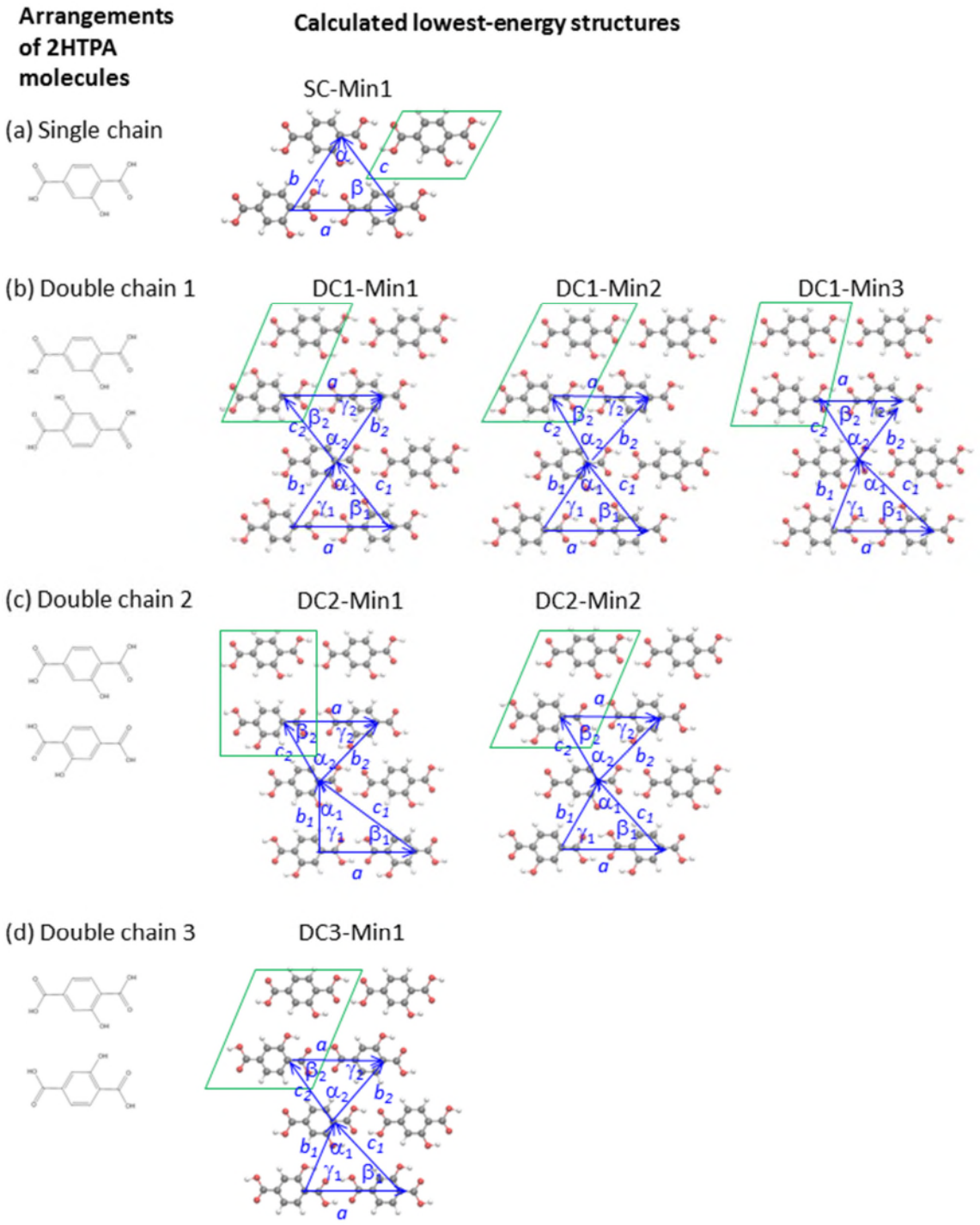

Figure 7. Single-chain and double-chain arrangements of 2HTPA molecules (left) and calculated lowest-energy structures of 2HTPA 2D monolayers (right). Lattice parameters are shown in blue. Unit cells are highlighted in green.

2HTPA. 2HTPA is a non-symmetric molecule containing one hydroxyl group. Therefore, unlike the symmetric TPA, 2HTPA can adsorb on a surface in four different orientations: with the hydroxyl group in the top-right, top-left, bottom-right, and bottom-left positions. While 2HTPA molecules within a chain display all the same orientation, molecules in neighbouring chains can be in each of these four orientations. This gives rise to four different arrangements for the 2HTPA molecular chains: a single-chain structure (SC, **Figure 7a**), where molecules have the same orientation over the entire monolayer, and three double-chain structures (DC, **Figures 7b-d**), where the orientations of the 2HTPA molecules in two adjacent chains differ. The packing of the molecular chains is uniform only in the former case (SC in **Figure 7a**), while different inter-chain distances result for all other cases, depending on the number and position of OH groups in between neighbouring molecules: 1 OH per molecular pair (DC2 in **Figure 7c**) or two OH between neighbouring chains followed by none in the successive pair (structures DC1, DC3 in **Figures 7b, d**).

The potential energy surfaces for the 2D monolayers of the single-chain and double-chain 2HTPA structures are shown in the Supporting Information, the lowest-energy structures are displayed in **Figure 7**, and the intermolecular distances in **Table 4**. While the unit cell of the SC structure contains only a single molecule, that of the DC structures comprises two molecules with two sets of inter-chain distances (described by b_1, c_1 and b_2, c_2) and two sets of angles (α_1, β_1, and α_2, β_2), reflecting the existence of two inter-chain arrangements.

A single minimum is found for the SC structure (a = 9.4 Å, b = 8.0 Å, γ = 51°, see **Table 4**), which is in good agreement with the experimentally observed regular 2HTPA monolayer (a = 9.7 Å, b = 8.4 Å, γ = 50°, see **Table 2**). In contrast, several minima are found for the double-chain structures. Notably, DC1-Min1, DC1-Min2 and DC2-Min1 are more stable than SC. This clearly shows that the 2HTPA molecule is capable of polymorphism. Moreover, the geometry of DC1-Min1 (the most stable calculated 2HTPA structure) is very similar to that of SC (distances within 0.3 Å, angles within 3°, i.e. differences below the ±5% accuracy of the experimental measurements). Thus DC1-Min1 is the most likely candidate structure for the experimentally observed regular 2HTPA monolayers.

The DC1-Min2 structure is only slightly less stable than DC1-Min1 (–82.3 vs –82.6 kJ mol^{-1}), but has a different arrangement of chains, resulting in alternating large and small inter-chain distances (both b_1, b_2 and c_1, c_2). Therefore, this structure is the most likely candidate for the observed alternating 2HTPA assembly (**Figure 5**). Among the other energy minima described in **Table 4**, one (DC2-Min2) also has the geometry similar to the alternating structure, but it is higher in energy, while the other minima are both high in energy and significantly different from the experimentally observed structures.

Therefore, two likely 2HTPA monolayer structures emerge: DC1-Min1 for the regular assembly, and DC1-Min2 for the alternating assembly. The very close similarity in energy of these two structures explains their experimentally observed coexistence. Moreover, the similarity in the monolayer binding energies also explains why this polymorphism of 2HTPA is not affected by the polar or apolar nature of the solvent. The specific pairing of 2HTPA molecular chains necessary for both DC1-Min1 and DC1-Min2 structures may also be the reason for the formation of molecular domains with different orientations (**Figures 3c**, **d** and **Figures 4a**, **b**): "wrong" molecular pairings may be encountered at grain boundaries.

25DHTPA. Since the 25DHTPA molecule has two OH groups, there are only two possible orientations it can take in adjacent chains: parallel and antiparallel, resulting in either single-chain or double-chain structures (**Figure 8**). Because of its symmetry, the PES of 25DHTPA is also much simpler than that of 2HTPA: only one minimum is found for the SC structure, and two minima for the DC structure, as presented in **Figure 8** and **Table 4**. The most stable structure, SC-Min1 (lattice parameters a = 9.4 Å, b = 8.3 Å, γ = 48°), is in very good agreement with the experimentally observed 25DHTPA monolayers in 7A (a = 9.3 Å, b = 8.4 Å, γ = 44°, **Table 2**).

The two DC structures are less stable than SC by ~8 kJ mol^{-1}, and the agreement with the experimental monolayer geometries in either 7A or in PO is not very good. However, both DC structures have a larger area per molecule than the SC structure (63.5-64.4 Å^2/molecule vs 58.3 Å^2/molecule), caused by the wider spacing between the chains. This sparser molecular packing is a characteristic of the experimental monolayers observed in PO, which have a larger area per molecule (65.5 Å^2/molecule) than those observed in 7A (55.6 Å^2/molecule). Thus, it is possible that the monolayers formed in PO are related to the calculated DC structures, in particular to DC-Min1, which matches better the experimentally observed uniform separation between the 25DHTPA chains. However, our force field was not able to fully reproduce the true structure of 25DHTPA chains in PO. The reason may be in the choice of the distance and energy parameters for the OH(phenol)···O(carboxylic) hydrogen bond: they was fitted to reproduce the strong intramolecular hydrogen bond in 2HTPA and 25DHTPA (see SI section S1), but this may also lead to the intermolecular OH(phenol)···O(carboxylic) hydrogen bonds being artificially shortened.

Overall, the 25DHTPA molecule appears to be capable of polymorphism, similarly to 2HTPA, although its lowest energy monolayer structure, SC-Min1, is clearly significantly more stable than the alternatives.

Figure 8. Single-chain and double-chain arrangements of 25DHTPA molecules (left) and calculated lowest-energy structures of 25DHTPA 2D

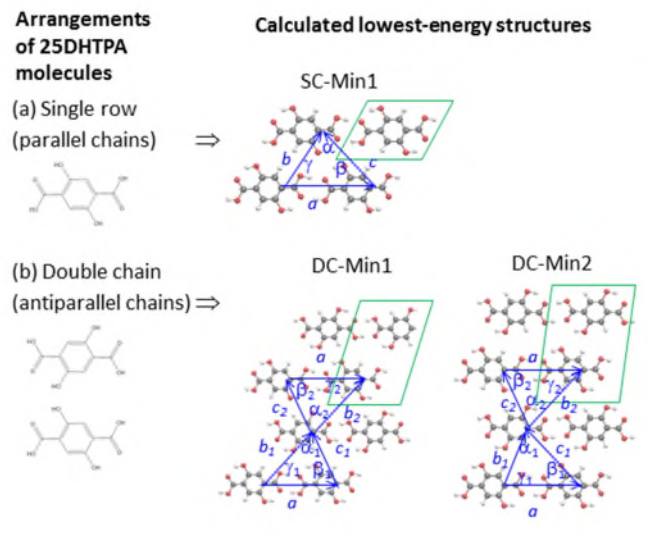

monolayers (right). Lattice parameters are shown in blue. Unit cells are highlighted in green.

3.3. Thermodynamic analysis of the self-assembly of substituted TPA

The calculations described above considered isolated monolayers, i.e. the effects of the substrate and the solvent were not explicitly included. To understand the nature of self-assembly at the solid-liquid interface, we need to take into account the fact that the molecules in a monolayer are adsorbed on a surface, are in contact with the solvent, and are in dynamic equilibrium with molecules dissolved in the solvent.

Born-Haber cycle. To achieve a quantitative description of the energetics of self-assembly at the solid-liquid interface and, in particular, of the effect of the solvent, we used the Born-Haber cycle (shown in **Figure 9** for TPA assembly at the HOPG/7A and HOPG/PO interfaces), similar to what done in Refs.[39, 56]

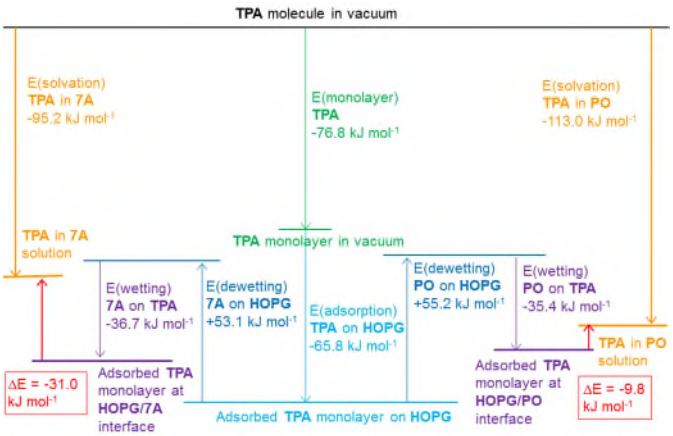

Figure 9. Born-Haber cycle for the self-assembly of TPA at the HOPG/7A and HOPG/PO interfaces. The energy of the monolayer formation at the solid/liquid interface, with respect to molecules in solution, is highlighted in red.

The energy of a monolayer of solute molecules adsorbed at the solid-liquid interface is calculated as a sum of several contributions: (i) the monolayer binding energy E_{ML}, i.e. the difference between the energy of a single isolated solute molecule and that of the same molecule within a monolayer; (ii) the adsorption energy E_{ads}, calculated as the binding energy of a single solute molecule on the graphite substrate; (iii) the de-wetting energy $E_{dewet} = E_{desorb(solv)} = -E_{ads(solv)}$, which accounts for the fact that the solvent, initially covering the substrate, needs to be desorbed to make space for the adsorption of the solute molecules; (iv) the wetting energy of the adsorbed monolayer $E_{wetting} = E_{ads(solv\text{-}on\text{-}ML)}$, that takes into consideration the fact that the monolayer of adsorbed solute molecules is in contact with a layer of solvent above it. Note that the latter two quantities, the energies of adsorption of the solvent on the substrate and on the monolayer, are calculated per 1 solvent molecule. On the other hand, the energetics of self-assembly is calculated per 1 molecule of solute. The solvent adsorption energies should therefore be re-scaled per area occupied by 1 solute molecule adsorbed on the substrate:[39]

$$E_{ads(solv)\,scaled} = E_{ads(solv)} / A_{solv} \times A_{solute} . \qquad (1)$$

Thus, the energy of monolayer assembly at the solid-liquid interface, $E_{ML@SLI}$, relative to that of a solute molecule in vacuum, is:

$$E_{ML@SLI} = E_{ML} + E_{ads} - E_{ads(solv)\,scaled} + E_{ads(solv\text{-}on\text{-}ML)\,scaled} . \qquad (2)$$

The energy of solvation $E_{solvation}$ is simply calculated as the difference between the energy of the system composed of one solute molecule within the solvent and the sum of the energies of the pure solvent and of the isolated solute molecule.

Finally, the energy gain (or cost) for the monolayer formation at the solid-liquid interface is the difference between the energy of the monolayer at the solid-liquid interface and the energy of solvation:

$$E_{monolayer\,formation} = E_{ML@SLI} - E_{solvation} . \qquad (3)$$

Table 5. Energies and areas per molecule involved in the Born-Haber cycle for TPA, 2HTPA and 25DHTPA at the HOPG/7A and HOPG/PO interfaces.

Molecule	Solvent	Area (solute) / Å^2	Area (solvent) / Å^2	$E_{solvation}$ / kJ mol^{-1}	E_{ML} / kJ mol^{-1}	E_{ads} / kJ mol^{-1}	$E_{ads(solv)}$ / kJ mol^{-1}	$E_{ads(solv)\ scaled}$ / kJ mol^{-1}	$E_{ads(solv-on-ML)}$ / kJ mol^{-1}	$E_{ads(solv-on-ML)\ scaled}$ / kJ mol^{-1}	$E_{ML@SLI}$ / kJ mol^{-1}	$E_{monolayer\ formation}$ / kJ mol^{-1}
TPA	7A	56.8	54.9	-95.2	-76.8	-65.8	-51.3	-53.1	-35.4	-36.7	-126.2	-31.0
TPA	PO	56.8	89.9	-113.0	-76.8	-65.8	-87.4	-55.2	-56.1	-35.4	-122.8	-9.8
2HTPA (DC Min1)	7A	57.8	54.9	-98.6	-82.6	-69.7	-51.3	-54.0	-41.8	-44.0	-142.3	-43.7
2HTPA (DC Min1)	PO	57.8	89.9	-114.3	-82.6	-69.7	-87.4	-56.2	-64.0	-41.1	-137.2	-22.9
25DHTPA (SC Min1)	7A	58.3	54.9	-93.8	-90.1	-75.4	-51.3	-54.5	-45.5	-48.3	-159.4	-65.6
25DHTPA (DC MIn1)	PO	63.5	89.9	-114.1	-82.2	-75.4	-87.4	-61.7	-66.5	-46.9	-142.8	-28.7
25DHTPA (SC Min1)	PO	58.3	89.9	-114.1	-90.1	-75.4	-87.4	-56.6	-66.5	-43.1	-152.0	-37.9

Energies. The energies of adsorption and solvation necessary for obtaining the monolayer formation energy have been calculated as described in the Computational Methods section (mean values of solvation energies over several MD simulations, and mean values of adsorption energies for a grid of adsorption positions above substrate), and are collected in **Table 5**. In particular, the calculated solvation energies are very similar between the three solute molecules, but vary with the solvent: –95.2 to –98.6 kJ mol^{-1} in 7A, –113.0 to –114.3 kJ mol^{-1} in PO. Interestingly, despite the possibility of strong hydrogen bond formation with the carboxylic groups of 7A, the solvation energies in PO are larger, showing that π-stacking in these systems is stronger than the hydrogen bonding. For comparison, the solvation energy of TPA in 9A calculated using the same method is –115.1 kJ mol^{-1}, and the experimental value is –114.4 kJ mol^{-1};[39] this is more than the solvation energies in 7A (–95.2 kJ mol^{-1}), showing that the dispersion interaction with the alkyl chains of the solvent is also non-negligible and is stronger for longer and more flexible alkyl chains. Note also that the variation (standard error of the mean) of the solvation energies is very large, up to $\pm$ 20.5 kJ mol^{-1} in PO and up to $\pm$41.9 kJ mol^{-1} in 7A, representing is the largest source of inaccuracy in our computational analysis.

Adsorption energies on HOPG progressively increase from TPA to 25DHTPA (from –65.8 to –75.4 kJ mol^{-1}, **Table 5**). Inspection of the potential energy surfaces of these molecules' adsorption shows that adsorption positions corresponding to AB stacking of the benzene ring above the underlying graphite are the most stable ones; however, the variation of energies between different adsorption positions is very small: the difference between the largest and smallest adsorption energy is only 1.1 kJ mol^{-1} for 25DHTPA, and 1.0 kJ mol^{-1} for 2HTPA (a similar difference of 0.8 kJ mol^{-1} between the adsorption minimum and maximum was found for TPA on HOPG previously[39]). This very flat potential energy surface for adsorption of these molecules on HOPG suggests that there is no strong preference towards specific adsorption positions.

The adsorption energy of PO on HOPG (–87.4 kJ mol^{-1}) is larger than that of 7A (–51.3 kJ mol^{-1}), in agreement with the area of the two solvent molecules and the presence/absence of phenyl rings. The difference in energies between adsorption maxima and minima is again small: 2.0 kJ mol^{-1} for PO, and 1.4 kJ mol^{-1} for 7A.

Adsorption of both solvents on monolayers is weaker than on HOPG (7A adsorption energies from –35.4 to –45.5 kJ mol^{-1}, PO adsorption energies from –56.1 to –66.5 kJ mol^{-1}, always strongest on 25DHTPA and weakest on TPA). This is as expected, because monolayers have a less dense structure than graphite and therefore fewer atoms to interact with. Interestingly, the variation in these adsorption energies is larger than on HOPG (standard deviation up to 6.4 kJ mol^{-1} for 7A adsorption and up to 4.0 kJ mol^{-1} for PO adsorption). This can be rationalised, as there are preferential positions both for 7A (the carboxylic group of 7A pointing towards the carboxylic and hydroxyl groups of TPA and its analogues) and PO (the phenyl ring of PO above the phenyl rings of TPA)

Analysis of the energetics of self-assembly. The energies summarised in **Table 5** can be combined according to equations (1)-(3) to calculate the energy gain for monolayer formation at the solid-liquid interface, which is presented in the extreme right column of **Table 5**. TPA is the most interesting example. The experiments show that TPA forms adsorbed self-assembled monolayers at the HOPG/7A interface but not at the HOPG/PO interface. The breakdown of the overall monolayer formation energy into contributions according to equations (1)-(3) is illustrated in **Figure 9.** Two of the contributions (the binding energy of the TPA monolayer in vacuum and the adsorption energy of a single TPA molecule on HOPG) are independent of the solvent, while the solvent wetting-dewetting processes stabilise the structure at the HOPG/7A interface slightly more than at the HOPG/PO interface. However, the biggest difference is in the solvation energies: solvation of TPA in PO is much more favourable than in 7A. As a result, the energy gain in forming the monolayer from solution in PO is very small (–9.8 kJ mol^{-1}) compared to 7A (–31.0 kJ mol^{-1}).

Note that the energies described here are enthalpies, while Gibbs free energies would be needed for a definitive answer whether adsorption from solution is possible or not. Thus,

although the self-assembly of TPA at the HOPG/PO interface still has a small enthalpic gain, this may be compensated by an entropic loss. The entropy of molecules in solution can be calculated[71] and in general depends on the structure of the molecule, concentration and temperature. For example, for TPA in 9A, the entropy term $-T\Delta S$ was estimated as $+3.4$ kJ mol^{-1},[39] and for a related slightly larger stilbenedicarboxylic molecule (SDA) as $+12.5$ kJ mol^{-1},[56] both values of similar magnitude to the enthalpy gain found here. Thus, the Gibbs free energy for this monolayer formation could be very close to zero, indicating that a stable adsorbed monolayer of TPA at the HOPG/PO interface should not form.

For TPA at the HOPG/7A interface and for all other 2HTPA and 25DHTPA systems considered here, the energy gain due to monolayer adsorption from solution (from -22.9 to -28.7 kJ mol^{-1} in PO and from -31.0 to -65.6 kJ mol^{-1} in 7A) is much larger than the entropy terms quoted above. Therefore, the Gibbs free energy for the self-assembly of these systems is always negative (favourable) – supported by the experimental observations of adsorbed monolayers. It can also be seen that the energy gain of self-assembly is always larger in 7A than in PO. This agrees with the experimentally observed full monolayer coverage in 7A and partial coverage in PO.

To summarise, the analysis of all energy contributions to the process of monolayer self-assembly at the solid-liquid interface enables us to explain the formation or absence of TPA monolayers in 7A and PO, respectively, and the differences in surface coverage of substituted TPA molecules at the interfaces between these solvents and HOPG.

Conclusions

Self-assembly of TPA and its hydroxylated analogues 2HTPA and 25DHTPA at the liquid/solid interfaces (graphite/heptanoic acid and graphite/1-phenyloctane) was studied using a combination of STM measurements and molecular mechanics and molecular dynamics calculations. The aim was to investigate the effects of the polar and apolar solvents on the self-assembly, and their interplay with weak (dispersion) and strong (hydrogen-bonding) interactions. STM results show that all three molecules form brickwork structures, similar to what was previously reported for TPA. However, the coverage achieved is different: full surface coverage is observed for all three molecules in 7A, partial coverage for 2HTPA and 25DHTPA in PO, and no adsorption of TPA in PO. There are further differences related to the nature of the molecules: the symmetric TPA and 25DHTPA form domains with a single orientation, while the non-symmetric 2HTPA forms multiply oriented domains. 2HTPA is also the only molecule that, besides the regular brickwork assembly, forms alternative structures characterised the pairing of H-bonded molecular chains with alternating small and large inter-chain separations. 25DHTPA forms two different brickwork structures depending on the solvent: a dense structure in 7A and a ~18% less dense structure in PO. Thus, polymorphism was observed, both induced by the solvent (for 25DHTPA) and related to the molecular structure (2HTPA).

To rationalise these results, molecular mechanics investigations of 2D monolayers of 2HTPA and 25DHTPA were carried out. 2D arrangements for both molecules had multiple minima, showing that both molecules should be capable of polymorphism. In particular, two 2D structures, close in energy but slightly different in geometry, were identified for 2HTPA, which correspond well to the regular and the alternating structures observed in the experiments. Because of the close similarity in their energies (only 0.3 kJ mol^{-1} preference for the "regular" structure), these structures are expected to co-exist independent of the solvent. For 25DHTPA, one energetically favoured 2D structure is found (attributed to the structure experimentally observed in 7A), as well as two less favourable structures, which may be the candidates for less dense structure experimentally observed in PO.

The energetics of self-assembly was explored by constructing the Born-Haber cycle and analysing the energy difference between adsorbed monolayers at the liquid-solid interface and molecules in solution. Solvation of all three molecules by PO was found more exothermic than solvation by 7A. For TPA at the HOPG/PO interface, the adsorbed and solvated systems were very close in energy, suggesting an equilibrium between molecular adsorption and molecules in solution, with no strong energetic preference for the TPA molecules to adsorb. By comparison, there is a strong preference for adsorption of TPA at the HOPG/7A interface, and for 2HTPA and 25DHTPA at both liquid/solid interfaces. The formation of an adsorbed monolayer is particularly favourable at the 7A interfaces, explaining why full monolayer coverage is achieved with this solvent but only partial coverage is observed in the PO solvent.

Thus, by studying the assembly of three very similar molecules, we obtained different outcomes: molecules self-assembling on a surface (forming a range of structures) or staying in solution. The outcome is controlled by a complex balance of solvent-solute, adsorbate-adsorbate and adsorbate-surface interactions. In the relatively simple model system studied here, the careful small changes in the molecules have allowed us to obtain a full insight in the causes behind the observed phenomenology, with an almost completely predictive model. That this is a very important result, demonstrating the level of control that an integrated experiment-theory approach can achieve in the technologically relevant field of molecular functionalisation of surfaces by 2D self-assembly.

Acknowledgements

RB and NM acknowledge the use of high-performance computing facilities provided by the University of Sheffield (Sol and Iceberg clusters). ADP was funded through a WPRS scholarship and an IAS early career fellowship of the University of Warwick. GC acknowledges financial support from the EU through the ERC Grant "VISUAL-MS".

References

‡ Electronic supplementary information (ESI) available. See DOI: ???/???

1. M. Gimenez-Marques, T. Hidalgo, C. Serre and P. Horcajada, *Coord. Chem. Rev.*, 2016, **307**, 342-360.
2. P. Xing and Y. Zhao, *Advanced Materials*, 2016, **28**, 7304-7339.
3. S. Casalini, C. A. Bortolotti, F. Leonardi and F. Biscarini, *Chemical Society Reviews*, 2017, **46**, 40-71.
4. K. W. Hipps, *Science*, 2001, **294**, 536.
5. S. R. Forrest, *Nature*, 2004, **428**, 911-918.
6. W. F. Smith, *Nat Nano*, 2007, **2**, 77-78.
7. N. Koch, *ChemPhysChem*, 2007, **8**, 1438-1455.
8. M. Fahlman, A. Crispin, X. Crispin, S. K. M. Henze, M. P. d. Jong, W. Osikowicz, C. Tengstedt and W. R. Salaneck, *Journal of Physics: Condensed Matter*, 2007, **19**, 183202.
9. E. Busseron, Y. Ruff, E. Moulin and N. Giuseppone, *Nanoscale*, 2013, **5**, 7098-7140.
10. D. M. Vriezema, M. Comellas Aragonès, J. A. A. W. Elemans, J. J. L. M. Cornelissen, A. E. Rowan and R. J. M. Nolte, *Chemical Reviews*, 2005, **105**, 1445-1490.
11. J. V. Barth, G. Costantini and K. Kern, *Nature*, 2005, **437**, 671-679.
12. J. V. Barth, *Annual Review of Physical Chemistry*, 2007, **58**, 345-407.
13. L. Dong, Z. A. Gao and N. Lin, *Prog. Surf. Sci.*, 2016, **91**, 101-135.
14. J. A. A. W. Elemans, S. Lei and S. De Feyter, *Angewandte Chemie International Edition*, 2009, **48**, 7298--7332.
15. M. Lackinger and W. M. Heckl, *Langmuir*, 2009, **25**, 11307-11321.
16. S. De Feyter and F. C. De Schryver, *Chemical Society Reviews*, 2003, **32**, 139-150.
17. T. Balandina, K. Tahara, N. Sändig, M. O. Blunt, J. Adisoejoso, S. Lei, F. Zerbetto, Y. Tobe and S. De Feyter, *ACS Nano*, 2012, **6**, 8381-8389.
18. M. O. Blunt, J. Adisoejoso, K. Tahara, K. Katayama, M. Van der Auweraer, Y. Tobe and S. De Feyter, *Journal of the American Chemical Society*, 2013, **135**, 12068-12075.
19. T. Sirtl, W. Song, G. Eder, S. Neogi, M. Schmittel, W. M. Heckl and M. Lackinger, *ACS Nano*, 2013, **7**, 6711-6718.
20. D. C. Y. Nguyen, L. Smykalla, T. N. H. Nguyen, T. Rüffer and M. Hietschold, *The Journal of Physical Chemistry C*, 2016, **120**, 11027-11036.
21. M. N. Nair, C. Mattioli, M. Cranney, J.-P. Malval, F. Vonau, D. Aubel, J.-L. Bubendorff, A. Gourdon and L. Simon, *The Journal of Physical Chemistry C*, 2015, **119**, 9334-9341.
22. G. M. Florio, B. Ilan, T. Müller, T. A. Baker, A. Rothman, T. L. Werblowsky, B. J. Berne and G. W. Flynn, *The Journal of Physical Chemistry C*, 2009, **113**, 3631-3640.
23. M. Lackinger, S. Griessl, W. M. Heckl, M. Hietschold and G. W. Flynn, *Langmuir*, 2005, **21**, 4984-4988.
24. L. Kampschulte, M. Lackinger, A.-K. Maier, R. S. K. Kishore, S. Griessl, M. Schmittel and W. M. Heckl, *The Journal of Physical Chemistry B*, 2006, **110**, 10829-10836.
25. W. Mamdouh, H. Uji-i, J. S. Ladislaw, A. E. Dulcey, V. Percec, F. C. De Schryver and S. De Feyter, *Journal of the American Chemical Society*, 2006, **128**, 317-325.
26. S.-L. Lee, Y.-C. Chu, H.-J. Wu and C.-h. Chen, *Langmuir*, 2012, **28**, 382-388.
27. N. T. N. Ha, T. G. Gopakumar and M. Hietschold, *Surface Science*, 2013, **607**, 68-73.
28. L. Cui, X. Miao, L. Xu, Y. Hu and W. Deng, *Physical Chemistry Chemical Physics*, 2015, **17**, 3627-3636.
29. S. Lei, K. Tahara, F. C. De Schryver, M. Van der Auweraer, Y. Tobe and S. De Feyter, *Angewandte Chemie International Edition*, 2008, **47**, 2964--2968.
30. N. Thi Ngoc Ha, T. G. Gopakumar and M. Hietschold, *The Journal of Physical Chemistry C*, 2011, **115**, 21743-21749.
31. X. Miao, L. Xu, Z. Li and W. Deng, *The Journal of Physical Chemistry C*, 2011, **115**, 3358-3367.
32. A. Ciesielski, P. J. Szabelski, W. Rżysko, A. Cadeddu, T. R. Cook, P. J. Stang and P. Samorì, *Journal of the American Chemical Society*, 2013, **135**, 6942-6950.
33. K. S. Mali, K. Lava, K. Binnemans and S. De Feyter, *Chemistry – A European Journal*, 2010, **16**, 14447--14458.
34. L. Xu, X. Miao, L. Cui, P. Liu, X. Chen and W. Deng, *Nanoscale*, 2015, **7**, 11734-11745.
35. X. Shen, X. Wei, P. Tan, Y. Yu, B. Yang, Z. Gong, H. Zhang, H. Lin, Y. Li, Q. Li, Y. Xie and L. Chi, *Small*, 2015, **11**, 2284--2290.
36. L. Cui, X. Miao, L. Xu and W. Deng, *Applied Surface Science*, 2014, **313**, 841-849.
37. J. M. MacLeod, O. Ivasenko, D. F. Perepichka and F. Rosei, *Nanotechnology*, 2007, **18**, 424031.
38. M. Lackinger, S. Griessl, L. Kampschulte, F. Jamitzky and W. M. Heckl, *Small*, 2005, **1**, 532-539.
39. W. T. Song, N. Martsinovich, W. M. Heckl and M. Lackinger, *Journal of the American Chemical Society*, 2013, **135**, 14854-14862.
40. M. Lackinger, S. Griessl, T. Markert, F. Jamitzky and W. M. Heckl, *The Journal of Physical Chemistry B*, 2004, **108**, 13652-13655.
41. R. Addou and M. Batzill, *Langmuir*, 2013, **29**, 6354-6360.
42. W. Zhang, A. Nefedov, M. Naboka, L. Cao and C. Woll, *Physical Chemistry Chemical Physics*, 2012, **14**, 10125-10131.
43. S. Clair, S. Pons, A. P. Seitsonen, H. Brune, K. Kern and J. V. Barth, *Journal of Physical Chemistry B*, 2004, **108**, 14585-14590.
44. T. Suzuki, T. Lutz, D. Payer, N. Lin, S. L. Tait, G. Costantini and K. Kern, *Physical Chemistry Chemical Physics*, 2009, **11**, 6498-6504.
45. Y.-G. Kim, S.-L. Yau and K. Itaya, *Langmuir*, 1999, **15**, 7810-7815.
46. S. L. Tait, Y. Wang, G. Costantini, N. Lin, A. Baraldi, F. Esch, L. Petaccia, S. Lizzit and K. Kern, *Journal of the American Chemical Society*, 2008, **130**, 2108-2113.
47. S. Stepanow, T. Strunskus, M. Lingenfelder, A. Dmitriev, H. Spillmann, N. Lin, J. V. Barth, C. Woll and K. Kern, *Journal of Physical Chemistry B*, 2004, **108**, 19392-19397.
48. Y. L. Wang, S. Fabris, G. Costantini and K. Kern, *Journal of Physical Chemistry C*, 2010, **114**, 13020-13025.
49. M. E. Cañas-Ventura, F. Klappenberger, S. Clair, S. Pons, K. Kern, H. Brune, T. Strunskus, W. Ch, R. Fasel and J. V. Barth, *The Journal of Chemical Physics*, 2006, **125**, 184710.
50. H. Aitchison, H. Lu, S. W. L. Hogan, H. Fruchtl, I. Cebula, M. Zharnikov and M. Buck, *Langmuir*, 2016, **32**, 9397-9409.
51. T. Suzuki, T. Lutz, G. Costantini and K. Kern, *Surface Science*, 2011, **605**, 1994-1998.

52. P. Rahe, M. Nimmrich, A. Nefedov, M. Naboka, C. Woll and A. Kuhnle, *Journal of Physical Chemistry C*, 2009, **113**, 17471-17478.
53. A. Tekiel, J. S. Prauzner-Bechcicki, S. Godlewski, J. Budzioch and M. Szymonski, *Journal of Physical Chemistry C*, 2008, **112**, 12606-12609.
54. P. Rahe, M. Nimmrich and A. Kuhnle, *Small*, 2012, **8**, 2969-2977.
55. J. M. MacLeod, J. A. Lipton-Duffin, D. Cui, S. De Feyter and F. Rosei, *Langmuir*, 2015, **31**, 7016-7024.
56. W. Song, N. Martsinovich, W. M. Heckl and M. Lackinger, *Physical Chemistry Chemical Physics*, 2014, **16**, 13239-13247.
57. I. Horcas, R. Fernández, J. M. Gómez-Rodríguez, J. Colchero, J. Gómez-Herrero and A. M. Baro, *Review of Scientific Instruments*, 2007, **78**, 013705.
58. J. W. Ponder and F. M. Richards, *Journal of Computational Chemistry*, 1987, **8**, 1016-1024.
59. N. L. Allinger, Y. H. Yuh and J. H. Lii, *Journal of the American Chemical Society*, 1989, **111**, 8551-8566.
60. J.-H. Lii and N. L. Allinger, *Journal of Computational Chemistry*, 1998, **19**, 1001-1016.
61. N. Martsinovich and A. Troisi, *Journal of Physical Chemistry C*, 2010, **114**, 4376-4388.
62. M. Head-Gordon, J. A. Pople and M. J. Frisch, *Chemical Physics Letters*, 1988, **153**, 503-506.
63. G. W. T. M. J. Frisch, H. B. Schlegel, G. E. Scuseria, M. A. Robb, J. R. Cheeseman, G. Scalmani, V. Barone, B. Mennucci, G. A. Petersson, H. Nakatsuji, M. Caricato, X. Li, H. P. Hratchian, A. F. Izmaylov, J. Bloino, G. Zheng, J. L. Sonnenberg, M. Hada, M. Ehara, K. Toyota, R. Fukuda, J. Hasegawa, M. Ishida, T. Nakajima, Y. Honda, O. Kitao, H. Nakai, T. Vreven, J. A. Montgomery, Jr., J. E. Peralta, F. Ogliaro, M. Bearpark, J. J. Heyd, E. Brothers, K. N. Kudin, V. N. Staroverov, R. Kobayashi, J. Normand, K. Raghavachari, A. Rendell, J. C. Burant, S. S. Iyengar, J. Tomasi, M. Cossi, N. Rega, J. M. Millam, M. Klene, J. E. Knox, J. B. Cross, V. Bakken, C. Adamo, J. Jaramillo, R. Gomperts, R. E. Stratmann, O. Yazyev, A. J. Austin, R. Cammi, C. Pomelli, J. W. Ochterski, R. L. Martin, K. Morokuma, V. G. Zakrzewski, G. A. Voth, P. Salvador, J. J. Dannenberg, S. Dapprich, A. D. Daniels, Ö. Farkas, J. B. Foresman, J. V. Ortiz, J. Cioslowski, and D. J. Fox, Gaussian, Inc., Wallingford CT, *Journal*, 2009.
64. Pubchem - Open Chemistry Database: Terephthalic Acid, https://pubchem.ncbi.nlm.nih.gov/compound/7489#section=Density, (accessed 02/03/2017).
65. Santa Cruz Biotechnology: 2-Hydroxyterephthalic Acid, https://www.scbt.com/scbt/product/2-hydroxyterephthalic-acid-636-94-2, (accessed 02/03/2017).
66. ChemBK Database: 2,5-dihydroxyterephthalic Acid, http://www.chembk.com/en/chem/2,5-dihydroxyterephthalic%20acid, (accessed 02/03/2017).
67. Pubchem - Open Chemistry Database: Heptanoic Acid, https://pubchem.ncbi.nlm.nih.gov/compound/8094#section=Density, 02/03/2017).
68. Sigma Aldrich: 1-Phenyloctane, http://www.sigmaaldrich.com/catalog/product/aldrich/113190?lang=en&region=GB, (accessed 02/03/2017).
69. M. Bailey and C. J. Brown, *Acta Crystallographica*, 1967, **22**, 387-391.
70. T. W. White, N. Martsinovich, A. Troisi and G. Costantini, unpublished work.
71. M. Mammen, E. I. Shakhnovich, J. M. Deutch and G. M. Whitesides, *The Journal of Organic Chemistry*, 1998, **63**, 3821-3830.